

AD-A263 573



PL-TR-93-2018

DTIC  
ELECTE  
MAY 5 1993  
S C D

2

**IONOSPHERIC STRUCTURE SPECIFICATIONS  
AND SYSTEMS EFFECTS**

**Sunanda Basu**

**Boston College  
Institute for Space Research  
Chestnut Hill, MA 02167**

**31 December 1992**

**Scientific Report No. 2**

**Approved for public release; distribution unlimited**




**PHILLIPS LABORATORY  
Directorate of Geophysics  
AIR FORCE MATERIEL COMMAND  
HANSCOM AIR FORCE BASE, MA 01731-3010**

93 5 04 004

**93-09439**



"This technical report has been reviewed and is approved for publication."

  
\_\_\_\_\_  
JAMES A. WHALEN  
Contract Manager

  
\_\_\_\_\_  
JOHN E. RASMUSSEN  
Branch Chief

  
\_\_\_\_\_  
WILLIAM K. VICKERY  
Division Director

This report has been reviewed by the ESC Public Affairs Office (PA) and is releasable to the National Information Service (NTIS).

Qualified requestors may obtain additional copies from the Defense Technical Information Center. All others should apply to the National Technical Information Service.

If your address has changed, or if you wish to be removed from the mailing list, or if the addressee is no longer employed by your organization, please notify PL/TSI, Hanscom AFB, MA 01731-3010. This will assist us in maintaining a current mailing list.

Do not return copies of this report unless contractual obligations or notices on a specific document requires that it be returned.

REPORT DOCUMENTATION PAGE			Form Approved OMB No 0704-0188	
Public reporting burden for this collection of information is estimated to average 1 hour per response, including the time for reviewing instructions, searching existing data sources, gathering and maintaining the data needed, and completing and reviewing the collection of information. Send comments regarding this burden estimate or any other aspect of this collection of information, including suggestions for reducing this burden, to Washington Headquarters Services, Directorate for Information Operations and Reports, 1215 Jefferson Davis Highway, Suite 1204, Arlington, VA 22202-4302, and to the Office of Management and Budget, Paperwork Reduction Project (0704-0188), Washington, DC 20503.				
1. AGENCY USE ONLY (leave blank)	2. REPORT DATE 31 DEC 92	3. REPORT TYPE AND DATES COVERED Scientific Report #2		
4. TITLE AND SUBTITLE Ionospheric Structure Specifications and Systems Effects		5. FUNDING NUMBERS PE 61102F PR 2310 TAG9 WU AM		
6. AUTHOR(S) Sunanda Basu		Contract: F19628-90-K-0007		
7. PERFORMING ORGANIZATION NAME(S) AND ADDRESS(ES) Boston College Institute for Space Research Chestnut Hill MA 02167		8. PERFORMING ORGANIZATION REPORT NUMBER		
9. SPONSORING/MONITORING AGENCY NAME(S) AND ADDRESS(ES) Phillips Laboratory 29 Randolph Road Hanscom AFB MA 01731-3010 Contract Manager: James Whalen/GPIA		10. SPONSORING/MONITORING AGENCY REPORT NUMBER PL-TR-93-2018		
11. SUPPLEMENTARY NOTES				
12a. DISTRIBUTION / AVAILABILITY STATEMENT Approved for public release; distribution unlimited		12b. DISTRIBUTION CODE		
13. ABSTRACT (Maximum 200 words) Ionospheric scintillation measurements are examined in relation to the satellite in-situ measurements of electron density structures in the ionosphere and the plasma processes responsible for the generation of these structures. Radio waves from satellites are scattered and ionospheric scintillation is recorded on the ground in the presence of a relative motion between the satellite, the ionosphere and the observer. The electron density irregularity spectrum of extended equatorial spread F structures, generated by Rayleigh-Taylor instability process, is found to be compatible with multi-frequency satellite scintillation measurements. In the case of equatorial bottomside sinusoidal irregularities, however, the power-law spectral index of scintillations is found to be considerably shallower than that expected. At high latitudes, two distinct classes of plasma instabilities, namely, the gradient-drift and shear-driven instability processes are identified. The observed difference of 0.5 between the spectral indices of high latitude scintillation and in-situ irregularity spectra has been explained in the context of anisotropic irregularity spectrum as postulated by Wernik et al. (1990).				
14. SUBJECT TERMS Ionospheric Scintillations VHF GHz Plasma Instabilities HF Heaters IMF Electron Density			15. NUMBER OF PAGES 34	
17. SECURITY CLASSIFICATION OF REPORT UNCLASSIFIED			16. PRICE CODE	
18. SECURITY CLASSIFICATION OF THIS PAGE UNCLASSIFIED		19. SECURITY CLASSIFICATION OF ABSTRACT UNCLASSIFIED		20. LIMITATION OF ABSTRACT UNLIMITED

## INTRODUCTION

Solar ultraviolet radiation and X-rays weakly ionize the upper atmospheric constituents to form the ionosphere which extends from an altitude of about 60 km to several thousand kilometers. The plasma density of the ionosphere is distributed non-uniformly in several layers, the lowermost D-region being formed at an altitude of about 85 km, the intermediate E-region at about 100 km and the F-region extends from about 150 km to several thousand kilometers. The bulk of the ionospheric plasma resides in the F-region, which attains its maximum plasma density at altitudes of 300 km. In the presence of the earth's magnetic field, the ionospheric plasma becomes magnetized. From the point of view of radio wave propagation, the ionosphere is thus described as a non-uniform, weakly ionized magnetoactive plasma.

The ionosphere often develops electron density structures which cover a wide range of scalelengths from a few centimeters to several thousand kilometers as illustrated in Figure 1. The large scalelengths are induced either by internal forcing functions, such as, planetary waves and gravity waves or external forcing functions such as the magnetospheric electric field at high latitudes. The small scalelength irregularities of electron density evolve due to a variety of plasma instabilities. Figure 1 shows that the wide range of scalelengths can only be studied by employing a variety of techniques, namely, the coherent and incoherent scatter radar, the digisonde, the scintillation recording systems, as well as the rocket and satellite in-situ probes.

In the present paper we shall concentrate on the intermediate scalelength range of electron density structures which are often called electron density irregularities due to their random characteristics. Transionospheric propagation of radio waves are markedly affected by the F-region irregularities since the electron content of the F-region predominates but, on occasions, the E-region irregularities may also affect the propagation. These electron density irregularities impose random phase fluctuations across the wavefront of a satellite signal that traverses the ionosphere. The emerging wavefront with phase fluctuations develop intensity fluctuations during its propagation to the ground and, as a result, spatial variations of intensity and phase develop on the ground. In the presence of a relative motion between the satellite, the ionosphere

and the observer on the ground, temporal variations of intensity and phase, known as intensity and phase scintillations are recorded by a receiver on the ground. For several decades, ionospheric scintillation observations have been made on a global scale which have contributed greatly to our understanding of the morphology of intermediate scale electron density irregularities (Aarons, 1982; Basu and Basu, 1981, 1985; Basu et al., 1988a). The theories of weak and strong ionospheric scintillation have been developed in the framework of wave propagation in a random medium (Tatarskii, 1961) by Rino (1979, 1980) and Yeh and Liu (1982 and references therein).

The objective of the present paper is to compare the electron density structures observed by satellite in-situ measurements with the structure of scintillation imposed by these irregularities on satellite signals. In addition the plasma instability mechanisms responsible for generating these ionospheric structures are discussed. In addition to the naturally occurring electron density irregularity structures, the structure of scintillation artificially induced by ground-based high-power high-frequency radio waves will also be discussed. The plan of the paper is as follows. In Section 1, the relationship between the one-dimensional irregularity spectrum obtained from satellite in-situ measurements and scintillation spectrum induced by these structures will be reviewed. In Section 2, we shall discuss the characteristics of equatorial F-region electron density structures observed in-situ by satellites in relation to the scintillation spectrum and the plasma instability mechanisms. In Section 3, the characteristics of scintillations induced by naturally occurring electron density irregularities will be compared with those artificially induced by high power, high frequency radio waves. In Section 4, the characteristics of electron density irregularity structures and scintillation in the high latitude ionosphere in the context of plasma instability mechanisms will be examined. Section 5 summarizes the results discussed in the paper.

# 1. IRREGULARITY SPECTRUM and SCINTILLATION SPECTRUM

The relationship between the three-dimensional electron density irregularity power spectrum and phase and intensity scintillation spectrum are given below. These were established by Cronyn (1970).

The three-dimensional wavenumber ( $k$ ) spectrum of electron density irregularities with a power law index of  $q$  and axial ratios  $\alpha$ ,  $\beta$  and  $\gamma$  along the three components of wavenumber  $\kappa_x$ ,  $\kappa_y$ , and  $\kappa_z$  can be expressed as

$$F_{ns}(k) \propto [1 + (\alpha\kappa_x)^2 + (\beta\kappa_y)^2 + (\gamma\kappa_z)^2]^{-q/2} \tag{1}$$

If a satellite-borne electron density probe scans through these irregularities in the x-direction with a velocity  $U$ , the temporal one-dimensional irregularity spectrum obtained from the space probe measurements may be given by

$$F_{ns}(v) = \frac{2\pi}{U} \int_{-\infty}^{+\infty} \int_{-\infty}^{+\infty} d\kappa_y d\kappa_z F_{ns}(2\pi v/U, \kappa_y, \kappa_z) \tag{2}$$

Under forward scatter approximation and for irregularity drift speed  $U$  in the x-direction, the temporal spectrum of phase scintillation is obtained as

DTIC QUALITY INSPECTION 5

$$F_{\phi}(v) = 2\pi(r_e\lambda)^2(L/U) \int_{-\infty}^{+\infty} d\kappa_y F_{ns}(2\pi v/U, \kappa_y, 0) \tag{3}$$

- where
- $v$  - the frequency,
  - $r_e$  - the classical electron radius,  $2.818 \times 10^{-15}$  m,
  - $\lambda$  - the radio wavelength in meters,
  - $L$  - the layer thickness of the irregularities in meters.

Accession For	
NTIS CRA&I	<input checked="" type="checkbox"/>
DTIC TAB	<input type="checkbox"/>
Unannounced	<input type="checkbox"/>
Justification	
By _____	
Distribution /	
Availability Codes	
Dist	Avail and/or Special
A-1	

The corresponding intensity scintillation spectrum is

$$F_{\phi}(\nu) = 2\pi(r_e\lambda)^2(L/U) \int_{-\infty}^{+\infty} d\kappa_y F_{ns}(2\pi\nu/U, \kappa_y, 0) \cdot \mathfrak{S}(2\pi\nu/U, \kappa_y) \quad (4)$$

where  $\mathfrak{S}(2\pi\nu/U, \kappa_y)$  - the Fresnel filter function.

Considering Eqs. (1) to (4), the high-frequency asymptotes of the spatial spectrum of the electron density irregularities and the temporal spectra of phase and intensity scintillations should be as shown in Figure 2 for  $q=4$ .

## 2. EQUATORIAL F-REGION IRREGULARITIES and SCINTILLATION

Figure 3 (Basu et al., 1988a) illustrates, with magnetic coordinate system, the global distribution of worst-case scintillation at low GHz (L-band) frequencies during the solar maximum and minimum conditions. The irregularities of electron density in the F-region of the ionosphere cause the observed scintillation. During the solar maximum period, scintillations are much enhanced due to increased background ionization density. The irregularity amplitude ( $\Delta N/N$ ) does not vary much with variation of solar activity, but the background ionization density varies by at least a factor of 10 from the solar maximum to the minimum period. The diagram shows that the major scintillation activity is concentrated around the magnetic equator in the pre-midnight period, in the auroral region during the nighttime period, and in the polar region at all local times.

The equatorial F-region irregularities are generated by the Rayleigh-Taylor instability mechanism (Dungey, 1956; Basu et al., 1978; Tsunoda, 1980, 1981; Kelley, 1989) after sunset when the eastward electric field is enhanced. The irregularities evolve in plume-like structures (Woodman and LaHoz, 1976), extend in altitude to more than 1000 km and, being field-aligned, encompass a nominal latitude range of  $\pm 15^\circ$  magnetic latitude. The plumes contain irregularities in the scalelength range of tens of kilometers to tens of centimeters. Figure 4 shows such plume structures being detected by radar backscatter at 50 MHz and 1.6 GHz scintillations at the magnetic equator.

The effect of these field-aligned plumes on scintillation activity is much enhanced at about  $15^\circ\text{N}$  and  $15^\circ\text{S}$  magnetic latitudes since the background ionization density is enhanced due to the transport of ionization from the magnetic equator. Scintillation measurements performed at such locations using multi-frequency transmissions from the Marisat satellite indicate (Figure 5) that even the scintillation index,  $S_4$ , at 1.54 GHz may attain a saturated level of 1.2 (Basu et al., 1987).

The satellite in-situ irregularity data acquired by the Atmospheric Explorer-E satellite at such locations of intense scintillation activity and its two slope ( $p_1 = -1.5$  and  $p_2 = -3.3$ ) spectrum



with a break scalelength of 750 m are illustrated in the bottom and the top panels of Figure 6 (Basu et al., 1983). A detailed description of the two slope irregularity spectrum obtained from satellite in-situ measurements may be obtained in the forthcoming publication of Livingston and Dabbs (1992). Similar two slope spectrum has been observed in rocket in-situ irregularity measurements (Rino et al., 1981; Kelley et al., 1982). Franke and Liu (1983) utilized two-slope in-situ irregularity power spectra obtained by Basu et al. (1983), and performed simulation studies to obtain multi-frequency scintillation spectra (Figure 7). Excellent agreement between the observations (Figure 5) and the simulation results (Figure 7) establishes the consistency between the in-situ irregularity spectrum and the scintillation spectrum in the framework of the scattering theory.

Equatorial irregularities causing scintillations are typically distributed over a layer of 200-km thickness around a mean altitude of 350 km. However, on occasions, the irregularities which are not fully developed, become confined within a thin layer in the bottomside F-region and exhibit sinusoidal spatial variations. The spatial structure and the spectrum of such bottomside sinusoidal structures (Valladares et al., 1983) detected by AE-E satellite in-situ measurements are shown in the top panel of Figure 8. The bottom panel shows that the corresponding scintillation spectra exhibit Fresnel oscillations as is to be expected in the case of weak scattering by a thin irregularity layer. It should, however, be noted that the one-dimensional irregularity spectral index of 5 indicated in the top panel does not correspond to the scintillation spectral index of 2.4 as illustrated in the bottom panel.

### 3. SCINTILLATIONS INDUCED BY HIGH-POWER HF HEATERS

The F-region irregularities may also be artificially induced by high power HF waves commonly called heaters (Erukhimov et al., 1979; Basu et al., 1987b; Frey et al., 1984). These artificial irregularities are excited by thermal forces (Fejer, 1979) in contrast to the natural irregularities which are generated by either homogeneous or inhomogeneous electric fields. The artificial irregularities attain their maximum amplitude 30 to 40 seconds after the heater is turned on and are quenched within one or two minutes after the heater is turned off. Figure 9 shows the locus of the 250-km subionospheric point of the ray path from a quasi-stationary polar beacon satellite transmitting at 250 MHz through the heater beam of the Max-Planck Institut für Aeronomie at Ramfjordmoen, Norway. The HF heater was operated at 5.1 MHz with an effective radiated power of 200 MW and was cycled 10 min on and 10 min off. The top and bottom panels of Figure 10 show the intensity and phase scintillation spectra during the fully developed state of scintillation. The intensity scintillation index corresponds to weak scintillations with  $S_4 = 0.12$ . The Fresnel oscillations are very evident in both the phase and intensity scintillation spectra and the Fresnel minima in the intensity scintillation spectra coincide with the Fresnel maxima of phase scintillation spectra. It indicates that the heater generated irregularities are confined to a layer with thickness less than 50 km. Model computations indicate that the irregularity amplitude,  $\delta n/n$ , is of the order of only 1%.

#### 4. HIGH LATITUDE SCINTILLATIONS

Scintillations at high latitudes are commonly observed in the nightside auroral oval above  $65^\circ$  corrected geomagnetic latitude (CGL) and within the polar cap located between  $75^\circ$  CGL and the magnetic pole. In the auroral oval, scintillations may be induced by irregularities generated locally by auroral particle precipitation, but much stronger irregularity structures convected from the polar cap may cause very intense scintillations (Tsunoda, 1988; Basu et al., 1991). Within the polar cap, the interplanetary magnetic field (IMF) dictates the type of plasma structures that are detected there (Buchau et al., 1985; Weber et al., 1984, 1986). These authors established that during a southward orientation of the interplanetary magnetic field, discrete patches of ionization, 1000 km in extent, with enhanced ionization density of the order of  $10^{12} \text{ m}^{-3}$  from midlatitudes are convected into the polar cap and then move in an antisunward direction and may enter the nightside auroral oval. On the other hand, when the IMF is northward, plasma structures oriented parallel to the noon-midnight direction develop due to particle precipitation and move in the dawn-dusk direction (Carlson, 1984). The influence of IMF on plasma structures observed within the polar cap is schematically illustrated in Figure 11. Basu et al. (1988b) showed that these patches of ionization develop small scale irregularities, which cause intense scintillations, due to the gradient drift instability mechanism as illustrated in the right-hand panel of Figure 11. The bottom diagram of the right-hand panel, adapted after the numerical simulation results of Mitchell et al. (1985), shows prominent protrusions or "fingers" of enhanced density growing outward from the boundary opposite to the direction of convection. At non-linear stages of development of the instability, the entire patch of ionization gets structured. On the other hand, the left-hand panel of Figure 11 shows that for the northward configuration of IMF, plasma gets structured at the edges of the arc due to velocity shear instability. The bottom panel, adapted after Keskinen et al. (1988) illustrates how the plasma gets structured by collisional Kelvin-Helmholtz instability mechanism.

The electron density irregularity structure and its spectrum for polar cap patches, obtained from DE-2 satellite in-situ measurements of electron density fluctuations (Basu et al., 1990a) is

illustrated by Figure 12. The spectrum shows that the one-dimensional irregularity spectrum between the scalelength range of 10 km to 250 m can be described by a spectral index of -1.9. Phase and intensity scintillation spectra for such patches of ionization obtained around the time of the in-situ measurements are shown in Figure 13. These measurements were made at Thule, Greenland, using the 250-MHz transmissions from the polar beacon satellite. The phase spectral slope, which is expected to reflect the in-situ spectra, is found to be -2.8 in good agreement with the one-dimensional in-situ spectral slope of -1.9. However, this agreement is an exception rather than the rule at high latitudes. The distribution of in-situ density irregularity and phase scintillation spectral slopes shown in Figure 14 indicates that the median value of the phase scintillation spectral index is -2.3 whereas for the one-dimensional in-situ density irregularity spectrum the index is -1.9. Such discrepancies have been examined by Wernik et al. (1990) in the context of anisotropic irregularity spectra and geometry of observations. It should be noted that the patches produce very intense scintillation primarily because the ionization density is so high. The major portion of the ionization density of the patches is not locally generated but reflects the high density of the sub-auroral ionosphere which is convected into the polar cap.

The irregularities in the arcs generated by the velocity shear instability mechanism have overall spectral slopes similar to that of the patches as shown by Basu et al. (1990b). However, the power spectral density of shear generated irregularities is higher at short scales and are more efficient in causing scintillations in the VHF range as established by Basu et al. (1986). In spite of this increased efficiency, the ionization density of the arcs, being locally generated by particle precipitation, is usually a factor of 5 less than the patches (Carlson et al., 1984). As a result, scintillations caused by the arcs are not as intense as that caused by the patches.

## 5. SUMMARY

Ionospheric scintillation studies seem to be based on a solid foundation since theoretical and experimental investigations of scintillations have been well coordinated with satellite in-situ measurements of irregularity structures and development of plasma instability theories generating such structures in the ionosphere.

Overall, there seems to be good agreement between satellite in-situ measurements of ionospheric structures, numerical simulation and field measurements. However, there remains discrepancies between in-situ irregularity and scintillation spectral slopes at high latitudes and at equatorial latitudes in the case of bottomside sinusoidal irregularities. The effects of anisotropic irregularity spectrum and observing geometry as discussed by Wernik et al. (1990) need to be investigated further.

## **ACKNOWLEDGMENT**

The work at Boston College was partially supported by PL contract F19628-90-0007.

## REFERENCES

- Aarons, J., Global morphology of ionospheric scintillation, *Proc. IEEE*, 70, 360, 1982.
- Basu S. and Su. Basu, Equatorial scintillations - a review, *J. Atmos. Terr. Phys.*, 43, 473, 1981.
- Basu, S., Su. Basu, J. Aarons, J.P. McClure, and M.D. Cousins, On the coexistence of kilometer- and meter-scale irregularities in the nighttime equatorial F region, *J. Geophys. Res.*, 83, 4219, 1978.
- Basu, S., E. MacKenzie, S. Basu, E. Costa, P.F. Fougere, H.C. Carlson, and H.E. Whitney, 250 MHz/GHz scintillation parameters in the equatorial, polar and auroral environments, *IEEE Journal on Selected Areas in Communications*, SAC-5, 102, 1987a.
- Basu, S., Su. Basu, P. Stubbe, H. Kopka, and J. Waaramaa, Daytime scintillations induced by high-power HF waves at Tromso, Norway, *J. Geophys. Res.*, 92, 11149, 1987b.
- Basu, S., E. MacKenzie, and Su. Basu, Ionospheric constraints on VHF/UHF communications links during solar maximum and minimum periods, *Radio Sci.*, 23, 363, 1988a.
- Basu, Su. and S. Basu, Equatorial scintillations: Advances since ISEA-6, *J. Atmos. Terr. Phys.*, 47, 753, 1985.
- Basu, Su., S. Basu, J.P. McClure, W.B. Hanson, and H.E. Whitney, High-resolution topside in-situ data of electron densities and VHF/GHz scintillations in the equatorial region, *J. Geophys. Res.*, 88, 403, 1983.
- Basu, Su., S. Basu, C. Senior, D. Weimer, E. Nielson, and P.F. Fougere, Velocity shears and subj-km scale irregularities in the nighttime auroral F-region, *Geophys. Res. Lett.*, 13, 101, 1986.

- Basu, Su., S. Basu, E.J. Weber, and W.R. Coley, Case study of polar cap scintillation modeling using DE-2 irregularity measurements at 800 km, *Radio Sci.*, 23, 545, 1988b.
- Basu, Su., S. Basu, E. MacKenzie, W.R. Coley, J.R. Sharber, and W.R. Hoegy, Plasma structuring by the gradient drift instability at high latitudes and comparison with velocity shear driven processes, *J. Geophys. Res.*, 95, 7799, 1990a.
- Basu, Su., S. Basu, E.J. Weber, and G.J. Bishop, Plasma structuring in the polar cap, *J. Geomag. Geoelectr.*, 42, 763, 1990b.
- Basu, Su., S. Basu, E. Costa, C. Bryant, C.E. Valladares, and R.C. Livingston, Interplanetary magnetic field control of drifts and anisotropy of high latitude irregularities, *Radio Sci.*, 26, 1079, 1991.
- Buchau, J., E.J. Weber, D.N. Anderson, H.C. Carlson, Jr., J.G. Moore, B.W. Reinisch, and R.C. Livingston, Ionospheric structures in the polar cap: their origin and relation to 250-MHz scintillation, *Radio Sci.*, 20, 325, 1985.
- Carlson, H.C., V.B. Wickwar, E.J. Weber, J. Buchau, J.G. Moore, and W. Whiting, Plasma characteristics of polar cap F-layer arcs, *Geophys. Res. Lett.*, 1, 895, 1984.
- Cronyn, W.M., The analysis of radio scattering and space probe observations of small-scale structure in the interplanetary medium, *Astrophys. J.*, 161, 755, 1970.
- Dungey, J.W., Convective diffusion in the equatorial F region, *J. Atmos. Terr. Phys.*, 9, 304, 1956.
- Erukhimov, L.M., V.I. Kovalev, A.M. Lerner, E.N. Myaskinov, I.N. Poddel'skii, and A.V. Rakhilin, Spectrum of large-scale artificial inhomogeneities in the F layer of the ionosphere, *Radio Phys. Quantum Electron., Engl. Trans.*, 22, 888, 1979.
- Fejer, J.A., Ionospheric modification and parametric instabilities, *Rev. Geophys.*, 17, 135, 1979.



- Franke, S.J. and C.H. Liu, Observations and modeling of multi-frequency VHF and GHz scintillations in the equatorial region, *J. Geophys. Res.*, **88**, 7075, 1983.
- Frey, A., P. Stubbe, and H. Kopka, First experimental evidence of HF produced electron density irregularities in the polar ionosphere: Diagnosed by UHF radio star scintillations, *Geophys. Res. Lett.*, **11**, 523, 1984.
- Kelley, M.C., J.F. Vickrey, C.W. Carlson, and R. Torbert, On the origin and spatial extent of high-latitude F-region irregularities, *J. Geophys. Res.*, **87**, 4469, 1982.
- Kelley, M.C., *The Earth's Ionosphere, Plasma Physics and Electrodynamics*, Academic Press Inc., San Diego, CA, p. 121, 1989.
- Keskinen, M.J., H.G., Mitchell, J.A. Fedder, P. Satyanarayana, S.T. Zalesak, and J.D. Huba, Nonlinear evolution of the Kelvin-Helmholtz instability in the high-latitude ionosphere, *J. Geophys. Res.*, **93**, 137, 1988.
- Livingston, R.C. and T.M. Dabbs, Observations of equatorial plasma irregularity spectrum, To be submitted to *Radio Sci.*, 1992.
- Mitchell, H.G., J.A. Fedder, M.J. Keskinen, and S.T. Zalesak, A simulation of high latitude F-layer instabilities in the presence of magnetosphere-ionosphere coupling, *Geophys. Res. Lett.*, **12**, 283, 1985.
- Rino, C.L., A power law phase screen model for ionospheric scintillation. 1. Weak scatter, *Radio Sci.*, **14**, 1135, 1979.
- Rino, C.L., Numerical computations for a one-dimensional power law phase screen, *Radio Sci.*, **15**, 41, 1980.

- Rino, C.L., R.T. Tsunoda, J. Petriceks, R.C. Livingston, M.C. Kelley, and K.D. Baker, Simultaneous rocket-borne beacon and in-situ measurements of equatorial spread-F intermediate wavelength results, *J. Geophys. Res.*, **86**, 2411, 1981.
- Tatarskii, V.I., *Wave Propagation in a Turbulent Medium*, McGraw-Hill Book Co., Inc., 1961.
- Tsunoda, R.T., Magnetic field-aligned characteristics of plasma bubbles in the nighttime equatorial ionosphere, *J. Atmos. Terr. Phys.*, **42**, 743, 1980.
- Tsunoda, R.T., Time evolution and dynamics of equatorial backscatter plumes. 1. Growth phase, *J. Geophys. Res.*, **86**, 139, 1981.
- Tsunoda, R.T., High-latitude F-region irregularities: a review and synthesis, *Rev. of Geophys.*, **26**, 719, 1988.
- Valladares, C.E., W.B. Hanson, J.P. McClure, and B.L. Cragin, Bottomside sinusoidal irregularities in the equatorial F region, *J. Geophys. Res.*, **88**, 8025, 1983.
- Weber, E.J., J. Buchau, J.G. Moore, J.R. Sharber, R.C. Livingston, J.D. Winningham, and B.W. Reinisch, F-layer ionization patches in the polar cap, *J. Geophys. Res.*, **89**, 1683, 1984.
- Weber, E.J., J.A. Klobuchar, J. Buchau, H.C. Carlson, Jr., R.C. Livingston, O. de la Beaujardiere, M. McCready, J.G. Moore, and G.J. Bishop, Polar cap F layer patches: structure and dynamics, *J. Geophys. Res.*, **91**, 12121, 1986.
- Wernik, A.W., C.H. Liu, S.J. Franke, and M. Gola, High-latitude irregularity spectra deduced from scintillation measurements, *Radio Sci.*, **25**, 883, 1990.
- Woodman, R.F. and C. LaHoz, Radar observations of F region equatorial irregularities, *J. Geophys. Res.*, **81**, 5447, 1976.

Yeh, K.C. and C.H. Liu, Radio wave scintillations in the ionosphere, *Proc. IEEE*, 70, 324, 1982.

## **FIGURE CAPTIONS**

- Figure 1. Variety of techniques used to study the wide range of scalelengths of electron density structures.
- Figure 2. The relationship of the three-dimensional electron density irregularity spectrum, the one-dimensional irregularity spectrum from space probe measurements, and the phase and intensity scintillation spectra.
- Figure 3. Global variation of scintillation fades during solar maximum and solar minimum conditions.
- Figure 4. (Top) Temporal variation of the range and intensity of 50-MHz radar backscatter observed at Jicamarca. (Bottom) Variation of the amplitude scintillation index ( $S_4$ ) of 1694-MHz signals from the geostationary satellites GOES-5 recorded at Ancon.
- Figure 5. A 3-min data segment of scintillations observed at 3954, 1541, and 257 MHz at Ascension Island and their respective spectra.
- Figure 6. A 3-sec sample of high resolution RPA data of relative amplitudes obtained on AE-E orbit 22759 on Dec 17, 1979 (lower panel). The upper panel shows a power spectrum of the linearly detrended data for this sample obtained by the FFT (dots) and maximum entropy (solid line) techniques.
- Figure 7. Multi-frequency temporal scintillation spectra computed from simulated scintillation data for the two-component power-law irregularity spectrum model (after Franke and Liu, 1983).

- Figure 8. The top panel shows the spatial structure and spectrum of a 3-sec interval of RPA data obtained on AE-E orbit 22700 during which bottomside sinusoidal structures were observed. The bottom panel shows the spectrum of LES-8 scintillation spectrum observed at this time from Huancayo, Peru.
- Figure 9. Geometry of observations indicating the half-power beamwidth (shaded region) of the HF heater and the locus of intersection of the ray path from Tromso to the polar beacon satellite with 250-km ionospheric height. The universal times are marked alongside the subionospheric track.
- Figure 10. The intensity and phase scintillation spectra during the full developed state of scintillation with Fresnel oscillations indicated.
- Figure 11. Influence of Interplanetary Magnetic Field (IMF) on plasma structures within the polar cap.
- Figure 12. Spectrum of one 8-sec sample of  $(\Delta N/N)_{rms}$  data from DE-2 satellite on March 8, 1982.
- Figure 13. Spectra of rms phase deviation (left panel) and intensity scintillation index  $S_4$  (right panel) from Thule on March 8, 1982.
- Figure 14. Histograms of (left panel) one-dimensional in-situ density spectral index,  $p_1$ , and (right panel) phase spectral index,  $p_\phi$ .

# HORIZONTAL SCALELENGTH

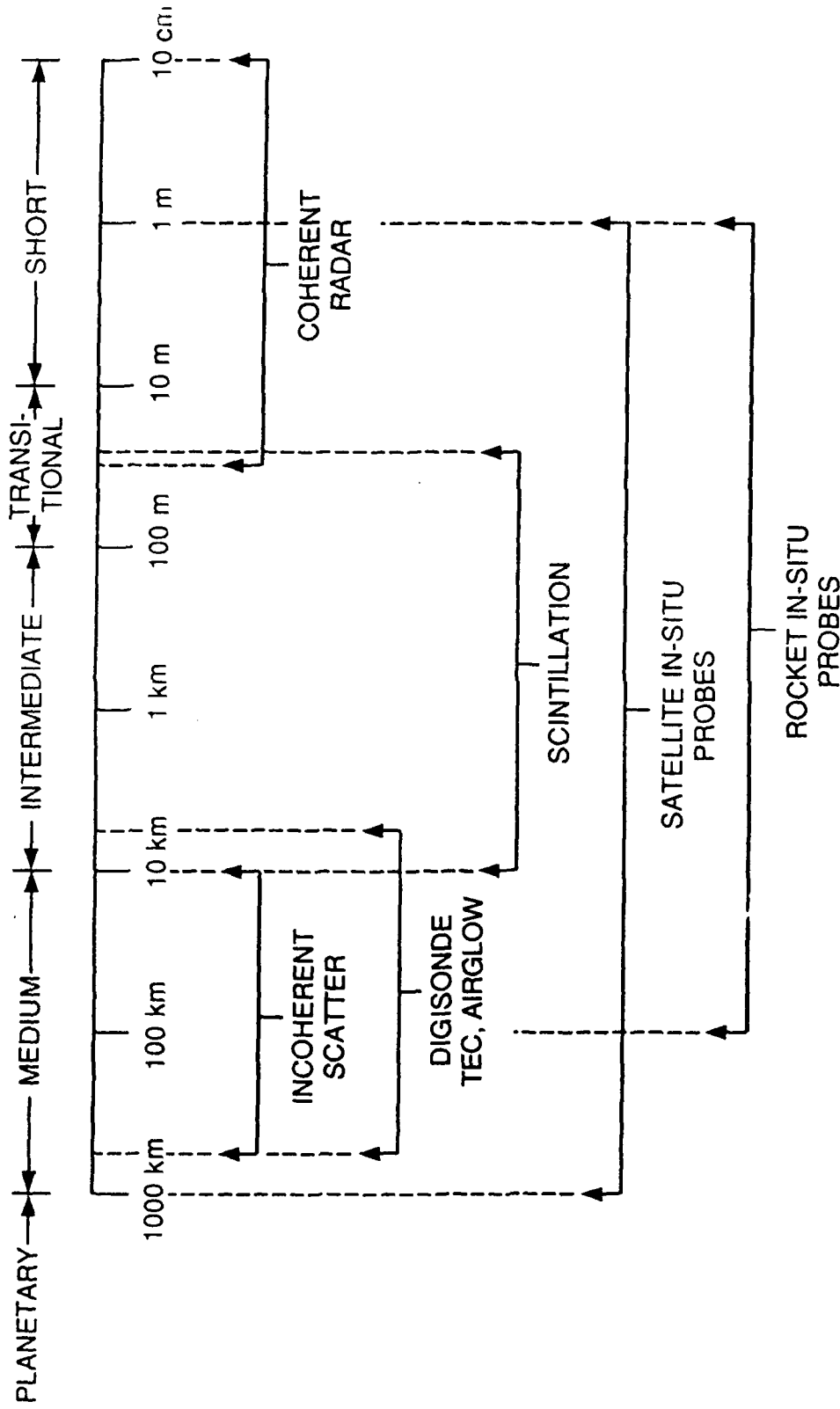
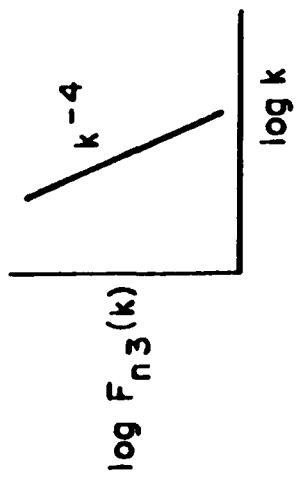
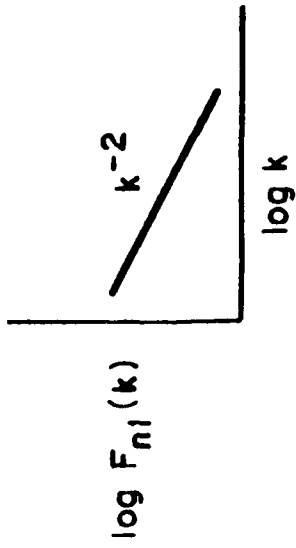


FIGURE 1

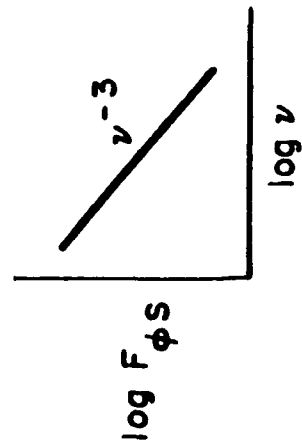
SPATIAL DENSITY  
3-D



SPATIAL DENSITY  
1-D



PHASE  
SCINTILLATION



INTENSITY  
SCINTILLATION

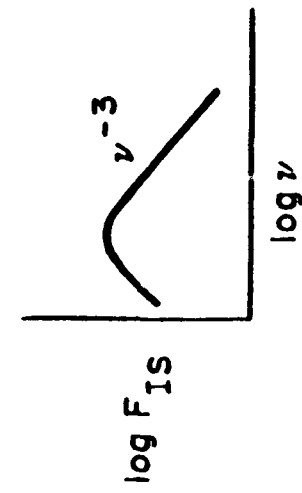


FIGURE 2

# "WORST CASE" FADING DEPTHS AT L-BAND

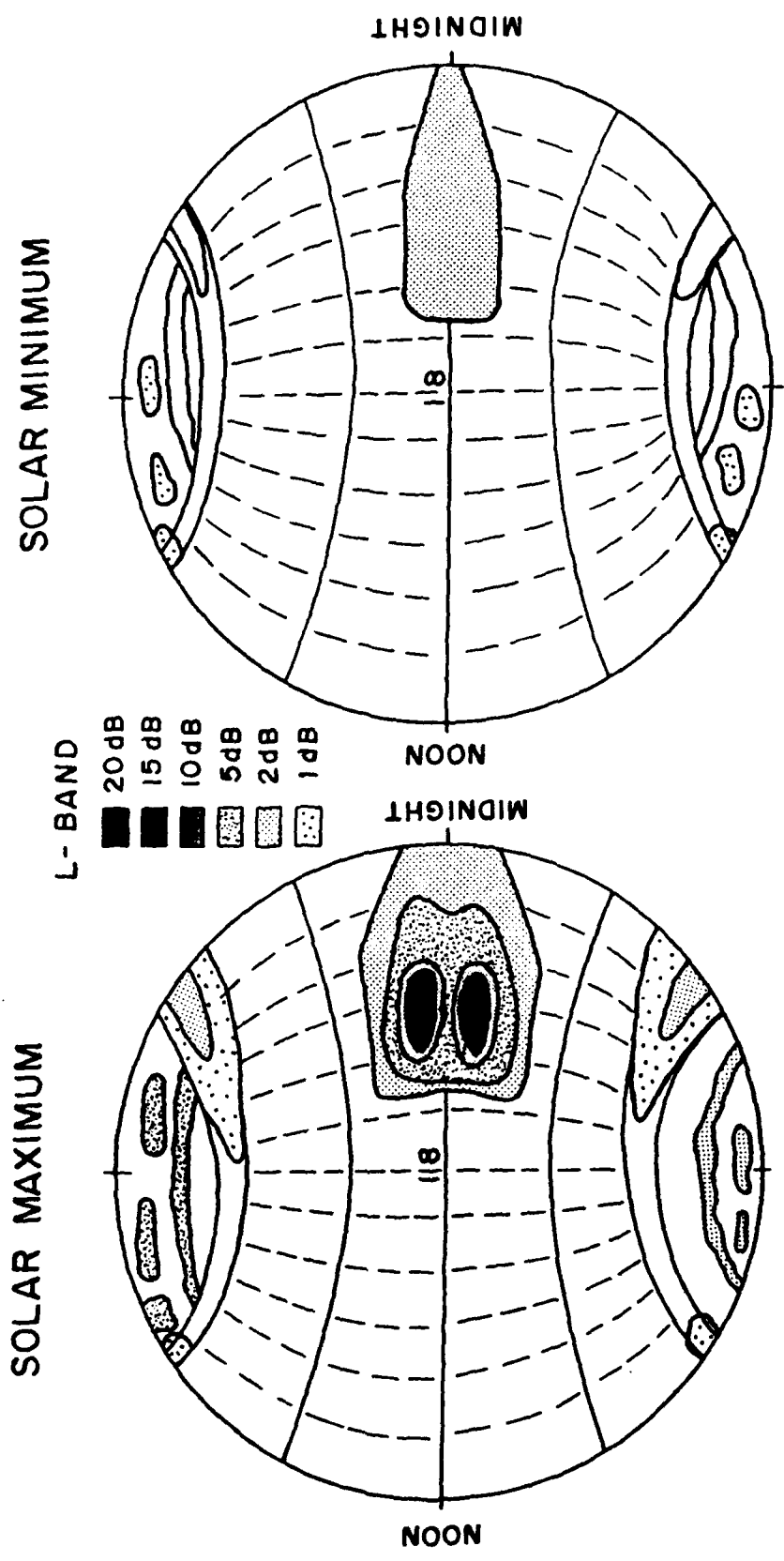


FIGURE 3



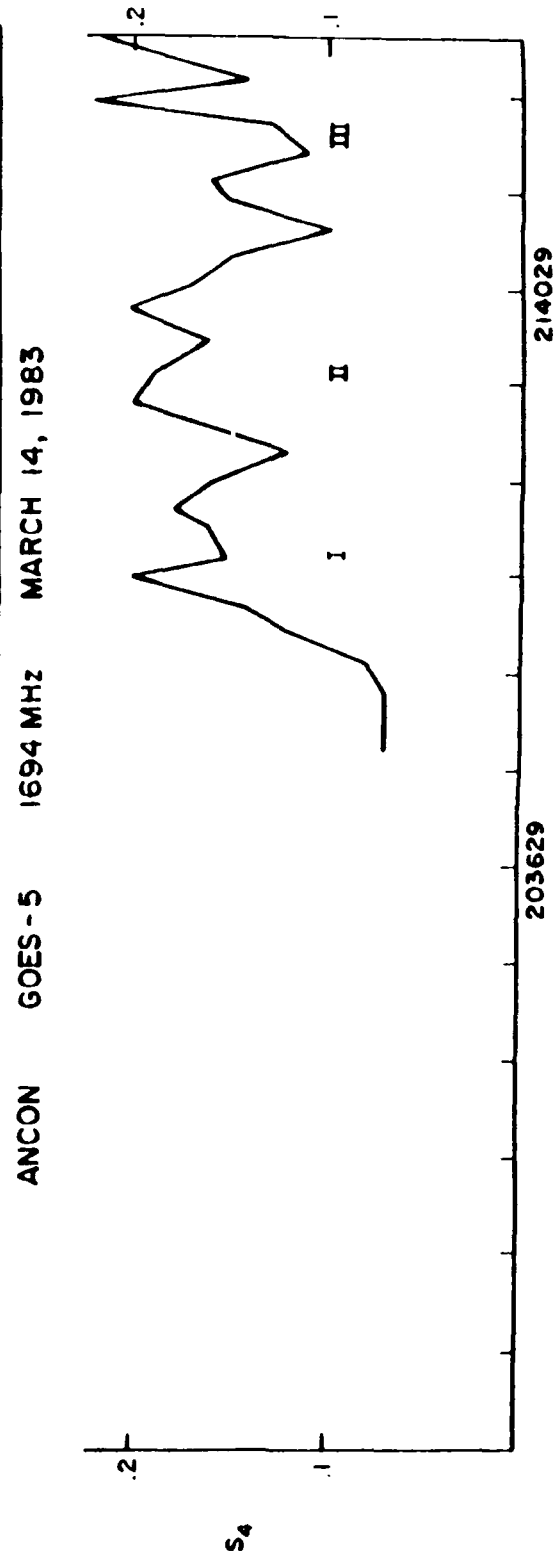
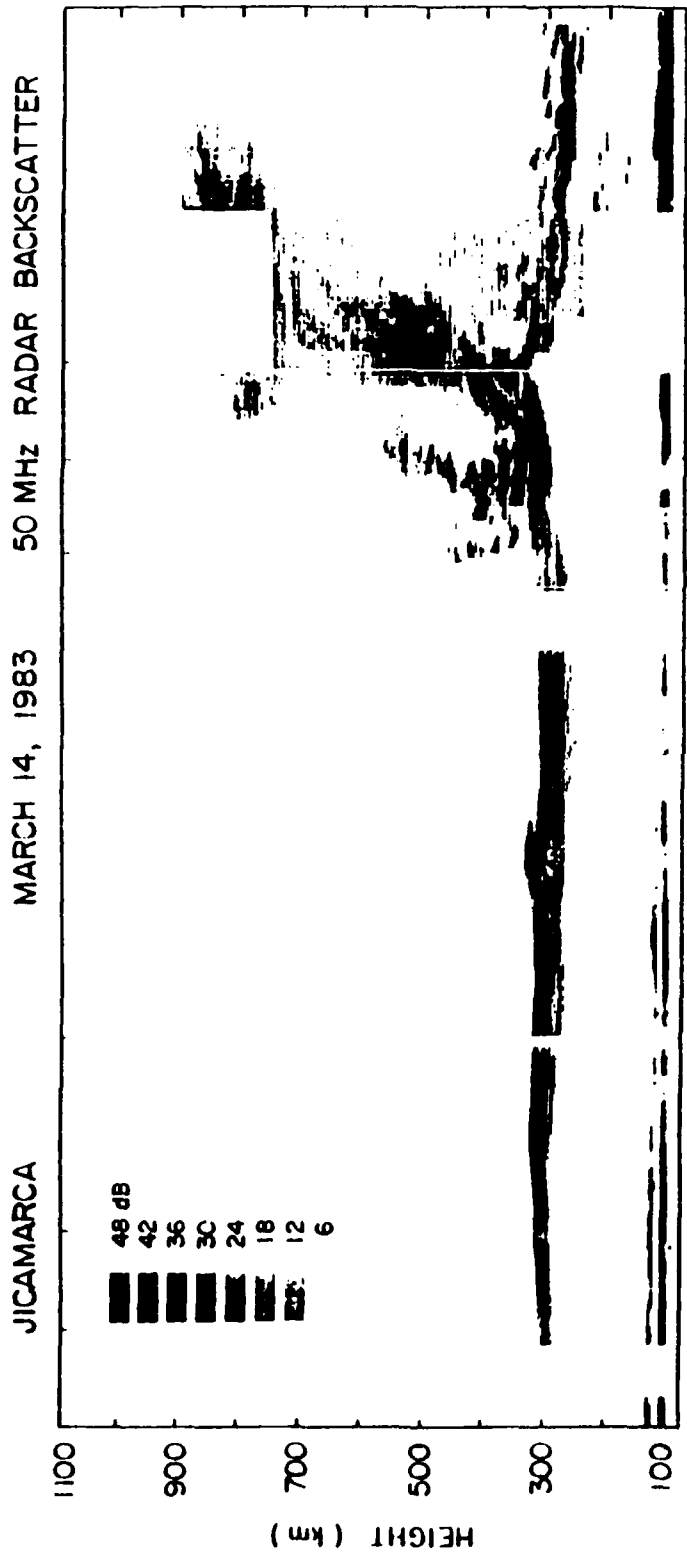


FIGURE 4

ASCENSION ISLAND  
FEB. 3, 1981  
2142 UT

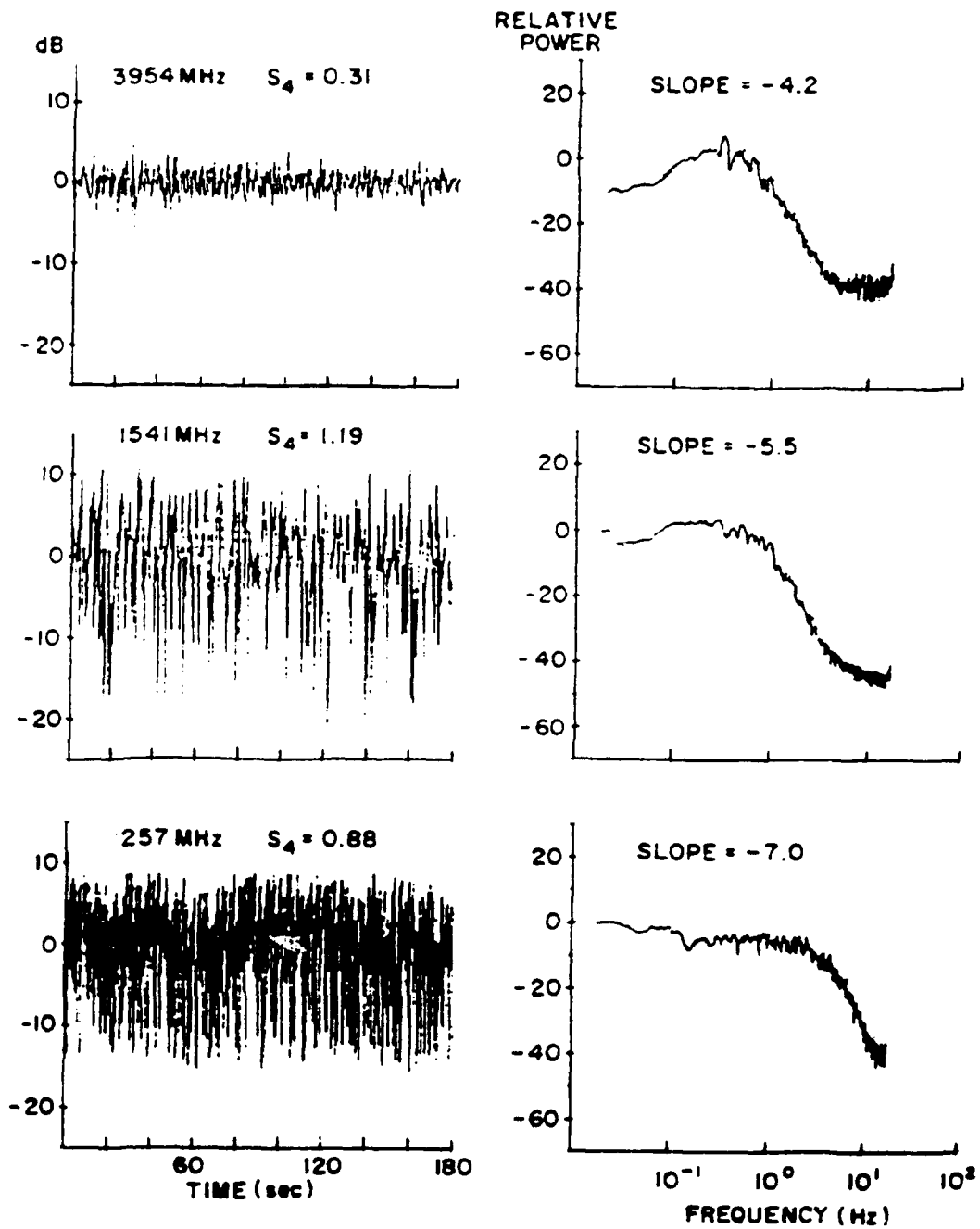


FIGURE 5

AE-E 22759  
 SIGMA % 13.694  
 NI 8.29E+05  
 ALT 436  
 SIN B.V 1.000  
 DIP -27.64  
 LONG -14.39  
 UT 003050

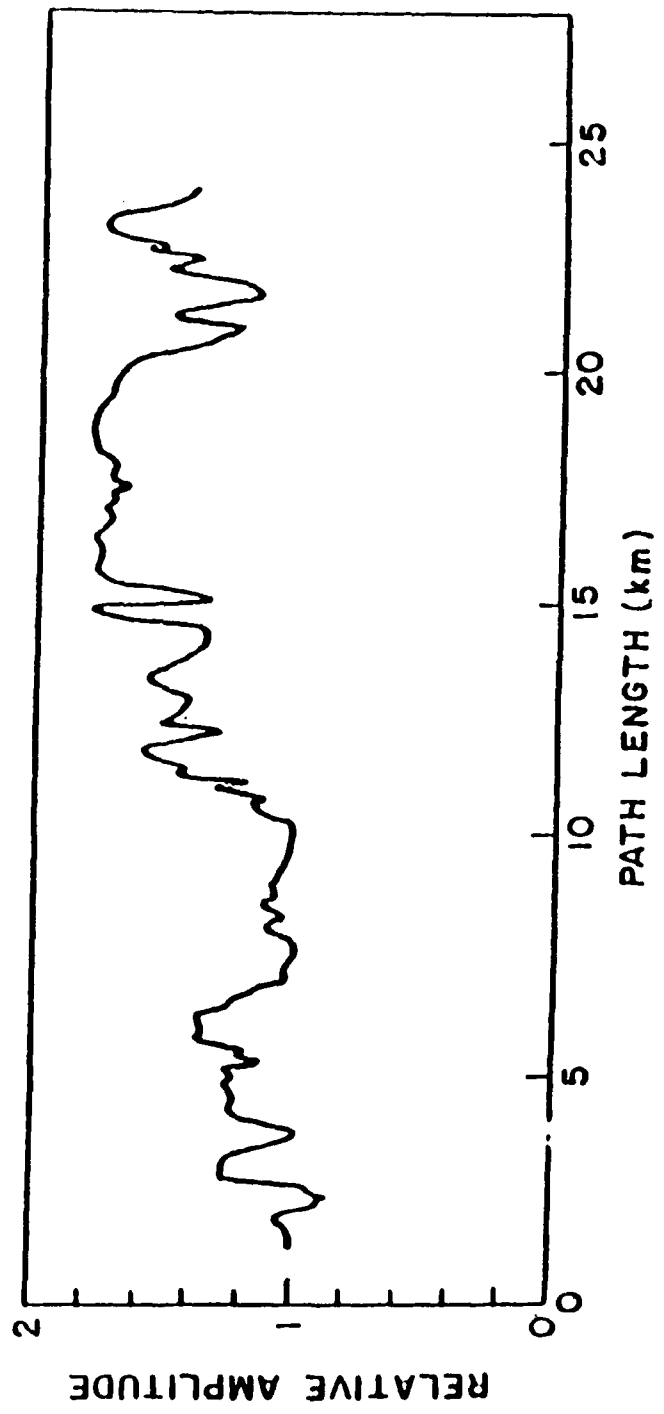
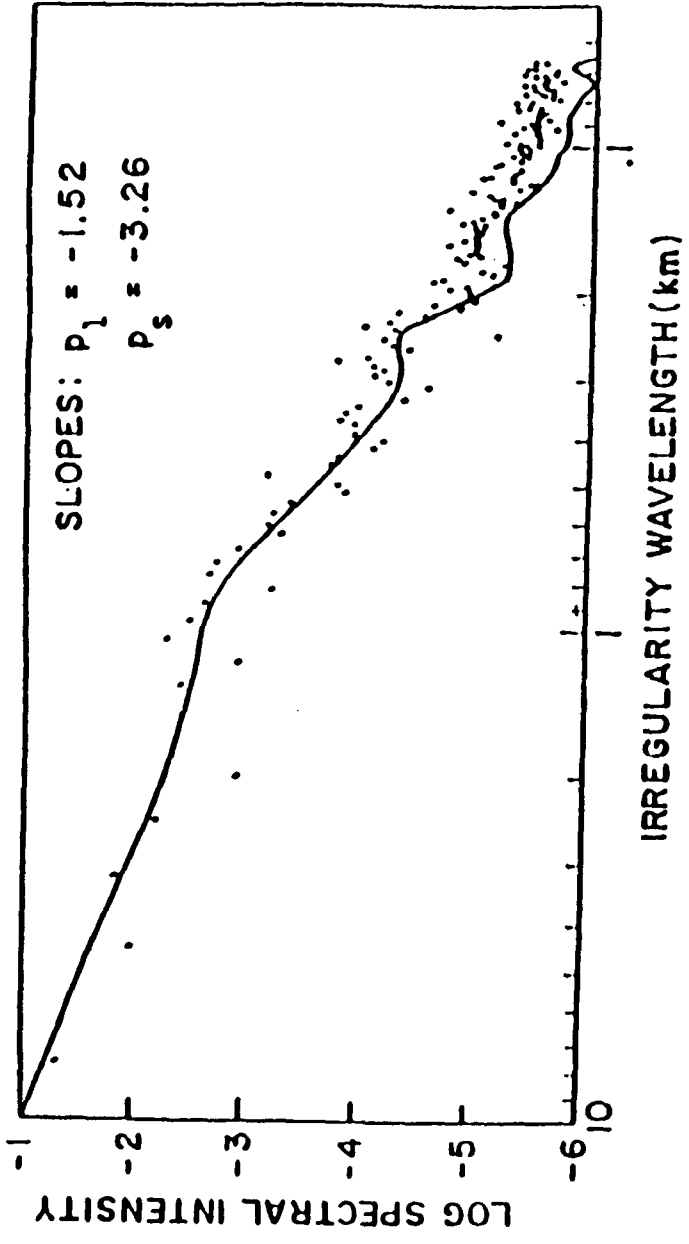


FIGURE 6

TWO COMPONENT MODEL

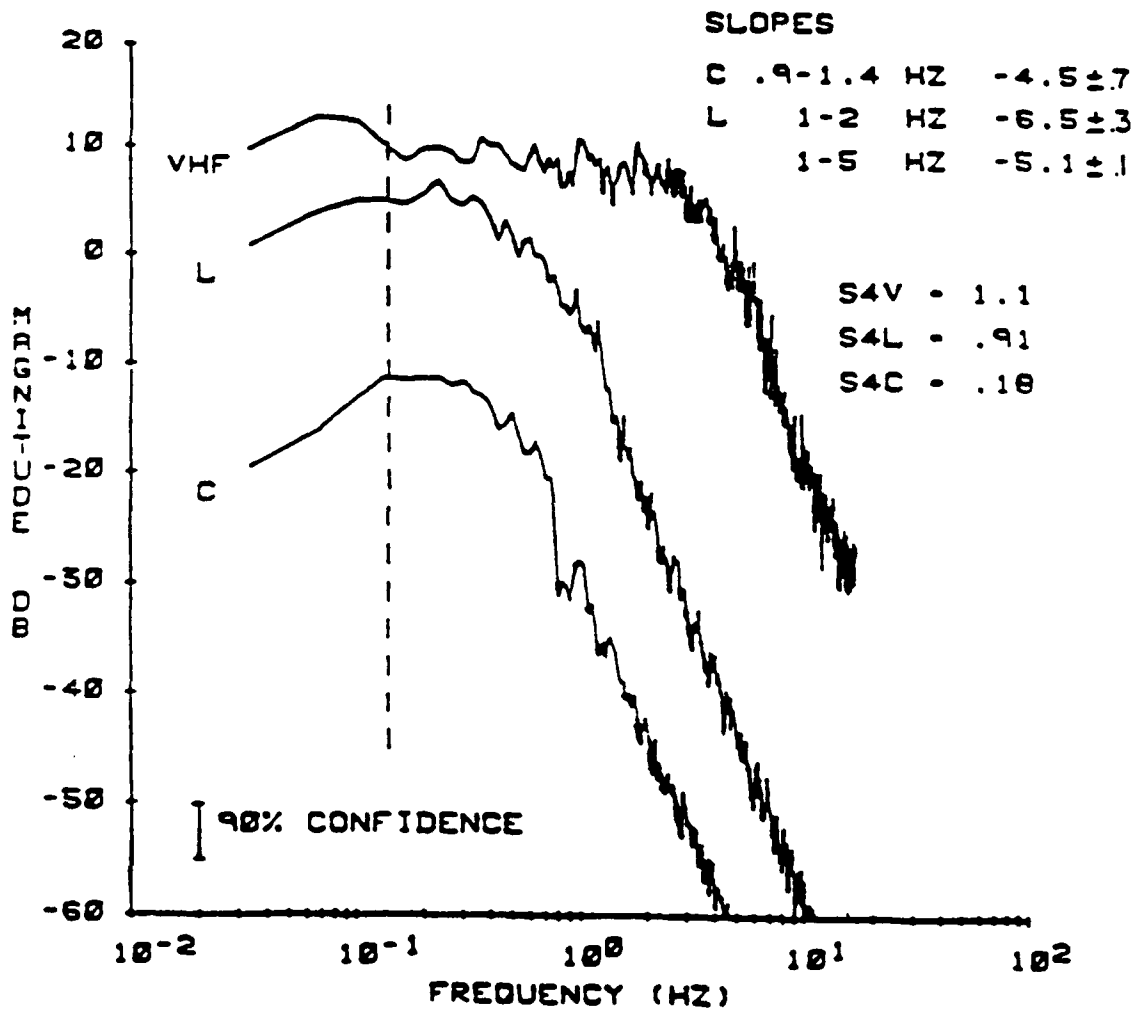
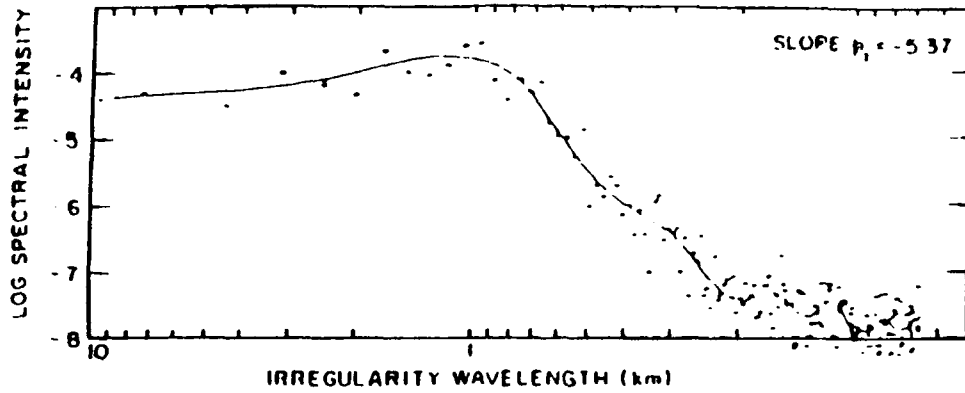


FIGURE 7



AE - E 22700  
 SIGMA % 3.5  
 NI 9.87E +04  
 UT 044930

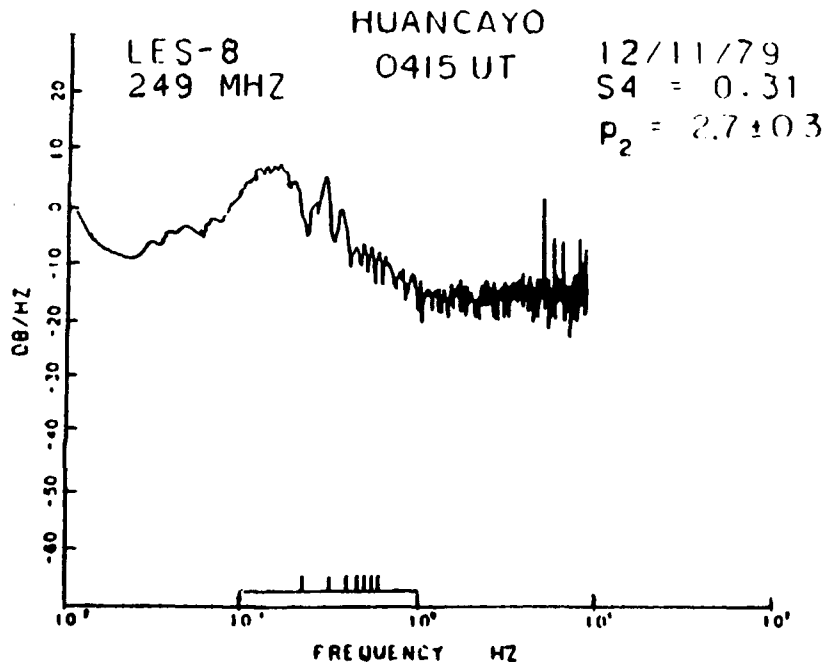
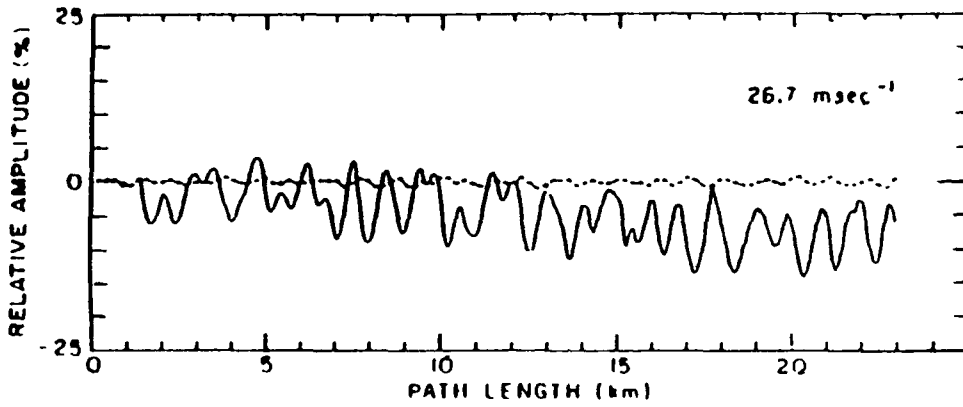


FIGURE 8

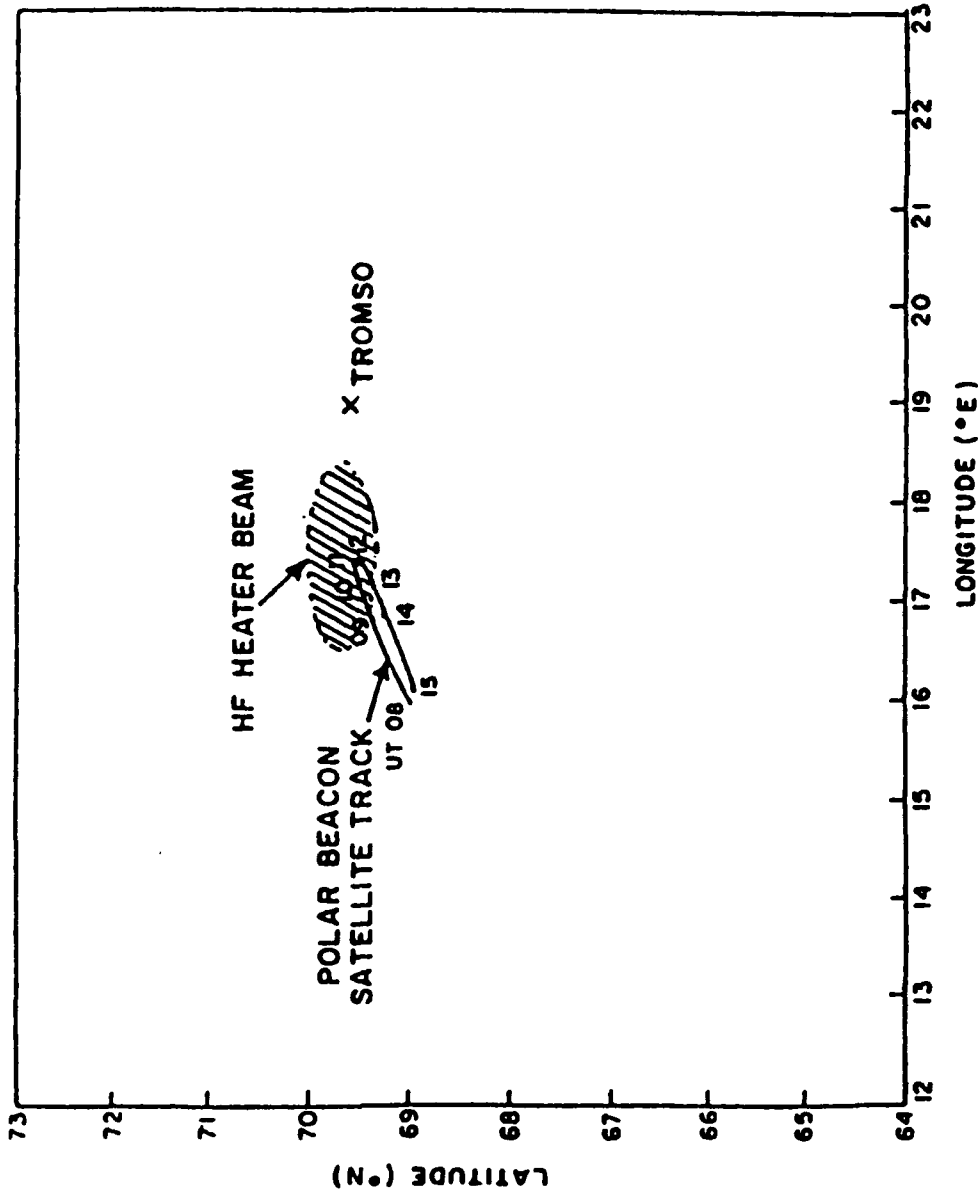


FIGURE 9

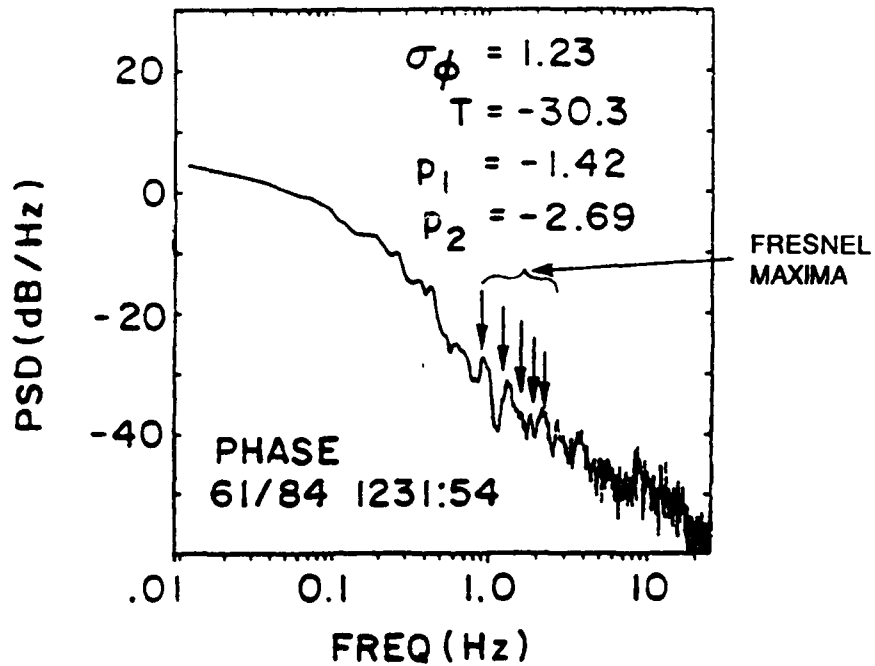
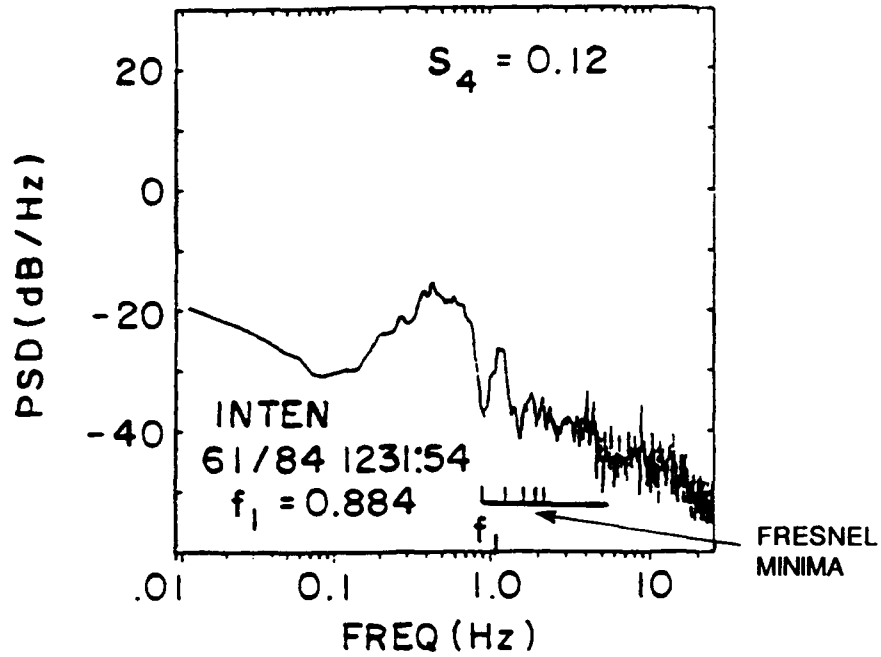
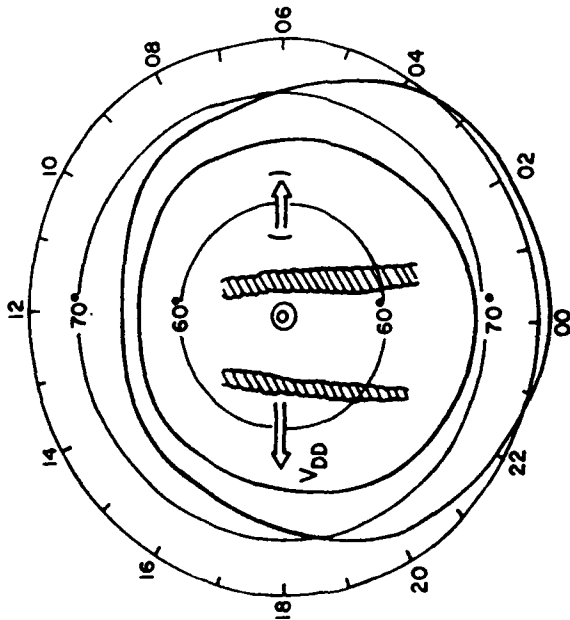


FIGURE 10

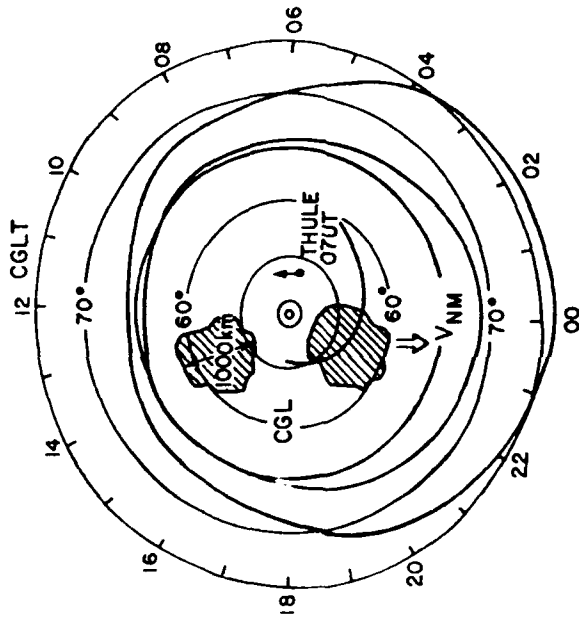
# POLAR CAP F-REGION STRUCTURES

IMF NORTHWARD  
 $B_z > 0$



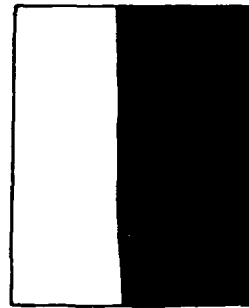
SUNALIGNED ARCS  
DAWN-DUSK DRIFT (PREDOMINANT)

IMF SOUTHWARD  
 $B_z < 0$



POLAR CAP PATCHES  
ANTI-SUNWARD DRIFT

SHEAR-DRIVEN INSTABILITY

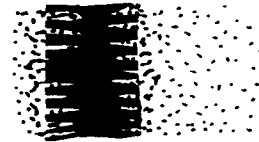


EARLY



LATE

GRADIENT-DRIFT INSTABILITY



EARLY



LATE

FIGURE 11



ORBIT 3223 82067  
 ION DENSITY 0344:07 UT

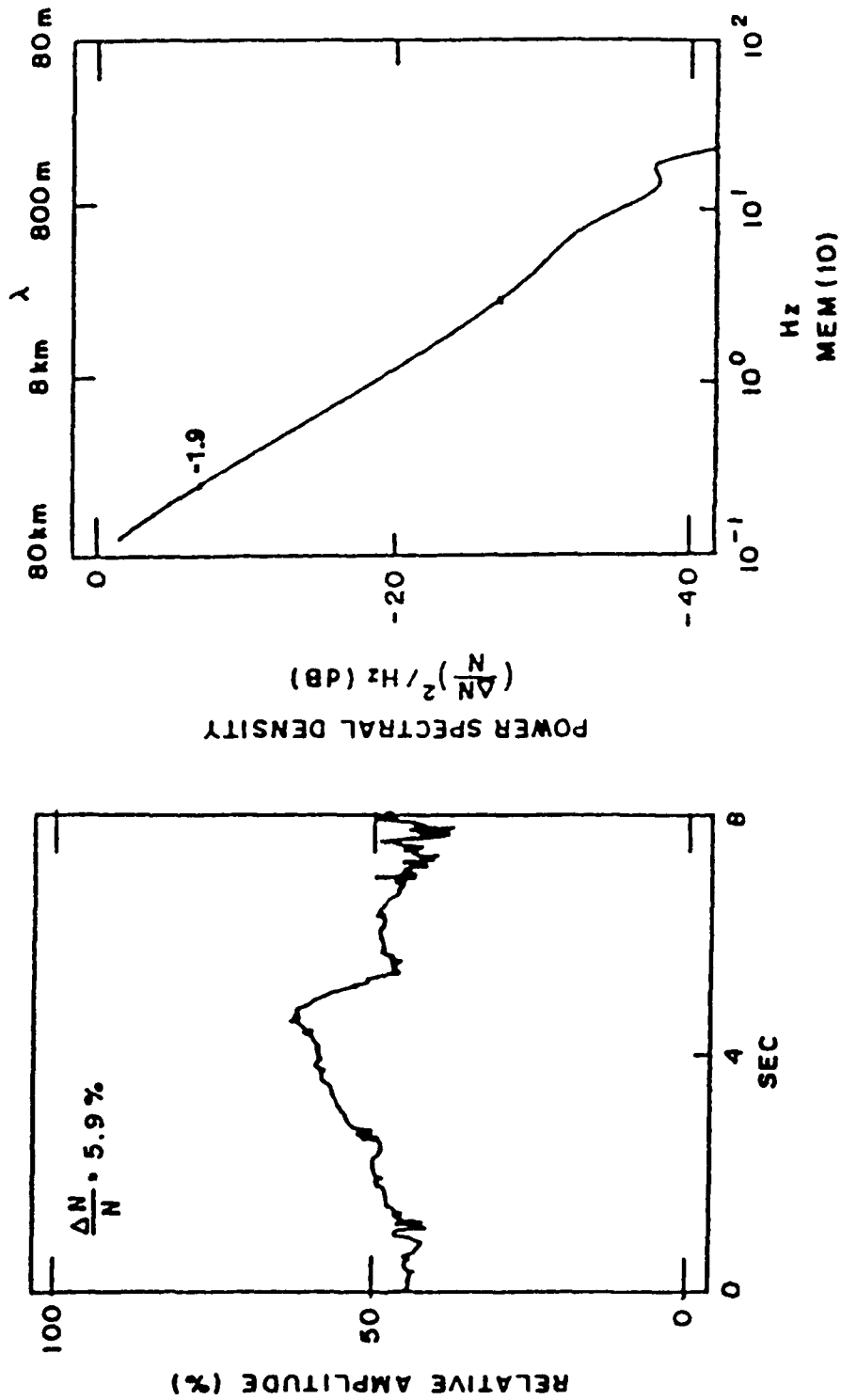


FIGURE 12

THULE MARCH 8, 1982  
042000 UT

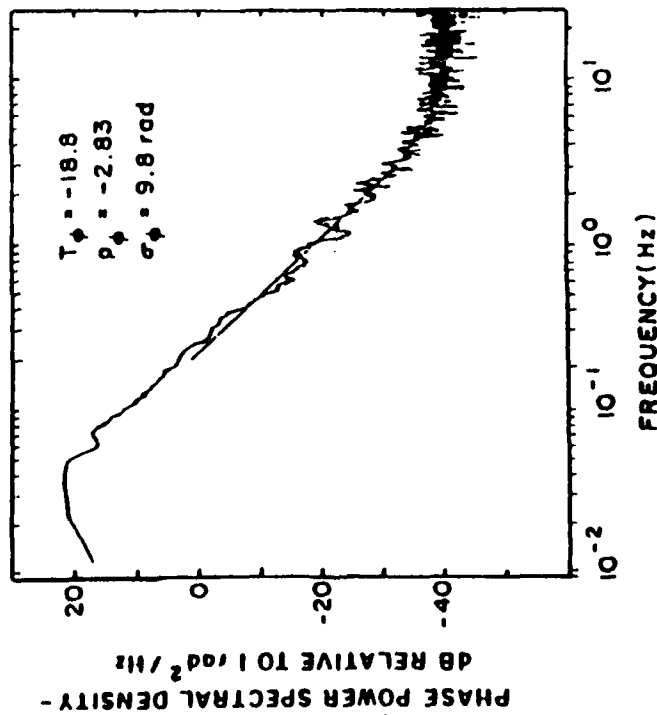
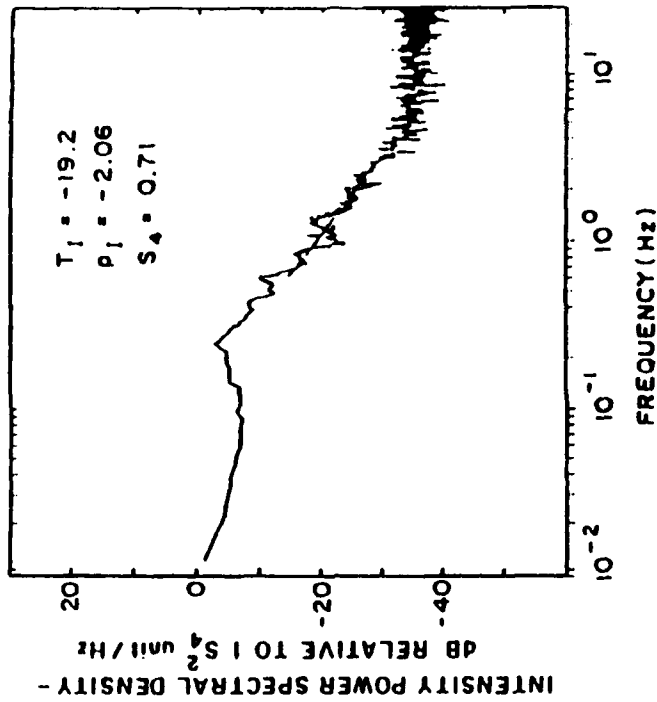
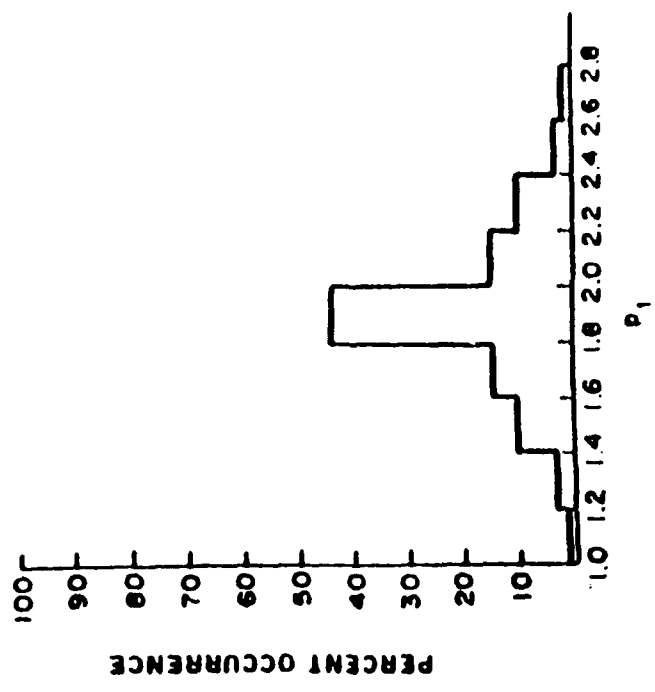


FIGURE 13

JAN. 22, 1982

DE-2 ORBIT 2550  
I-D DENSITY SPECTRA  $P_1$   
0650-0700UT 73pis



JAN. 22, 1982  
THULE POLAR BEACON  
PHASE SCINTILLATION SPECTRA  $P_4$   
0711-1312UT  
 $S_4 = .3 - .6$

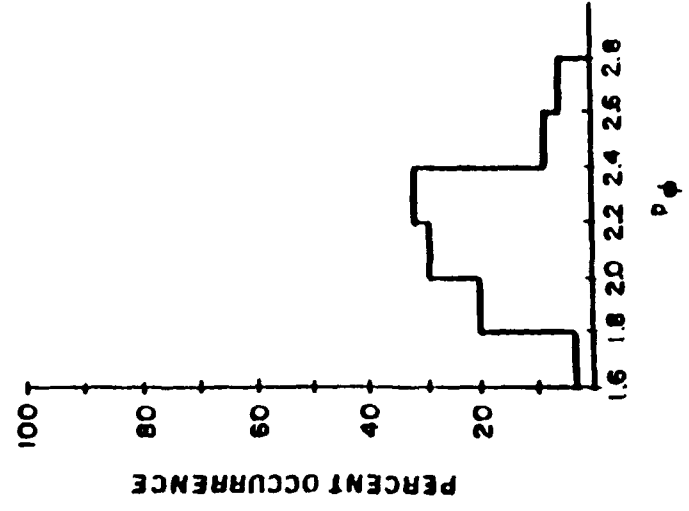


FIGURE 14